Atmos. Chem. Phys., 18, 16601–16618, 2018
https://doi.org/10.5194/acp-18-16601-2018

Atmospheric Chemistry and Physics
Open Access
EGU

Vertical and horizontal distribution of regional new particle formation events in Madrid

Cristina Carnerero[1,2], Noemí Pérez[1], Cristina Reche[1], Marina Ealo[1], Gloria Titos[1], Hong-Ku Lee[3], Hee-Ram Eun[3], Yong-Hee Park[3], Lubna Dada[4], Pauli Paasonen[4], Veli-Matti Kerminen[4], Enrique Mantilla[5], Miguel Escudero[6], Francisco J. Gómez-Moreno[7], Elisabeth Alonso-Blanco[7], Esther Coz[7], Alfonso Saiz-Lopez[8], Brice Temime-Roussel[9], Nicolas Marchand[9], David C. S. Beddows[10], Roy M. Harrison[10,11], Tuukka Petäjä[4], Markku Kulmala[4], Kang-Ho Ahn[3], Andrés Alastuey[1], and Xavier Querol[1]

[1]Institute of Environmental Assessment and Water Research (IDAEA-CSIC), Barcelona, 08034, Spain
[2]Department of Civil and Environmental Engineering, Universitat Politècnica de Catalunya, Barcelona, 08034, Spain
[3]Department of Mechanical Engineering, Hanyang University, Seoul, Republic of Korea
[4]Department of Physics, University of Helsinki, Helsinki, 00560, Finland
[5]Centro de Estudios Ambientales del Mediterráneo, CEAM, Paterna, 46980, Spain
[6]Centro Universitario de la Defensa de Zaragoza, Academia General Militar, Zaragoza, 50090, Spain
[7]Department of Environment, Joint Research Unit Atmospheric Pollution, CIEMAT, Madrid, 28040, Spain
[8]Department of Atmospheric Chemistry and Climate, Institute of Physical Chemistry Rocasolano (IQFR-CSIC), Madrid, 28006, Spain
[9]Aix Marseille Univ, CNRS, LCE, Marseille, 13003, France
[10]National Centre for Atmospheric Science, University of Birmingham, Birmingham, B15 2TT, UK
[11]Department of Environmental Sciences, Centre for Excellence in Environmental Studies, King Abdulaziz University, Jeddah, 21589, Saudi Arabia

Correspondence: Cristina Carnerero (cristina.carnerero@idaea.csic.es)

Received: 15 February 2018 – Discussion started: 27 March 2018
Revised: 29 October 2018 – Accepted: 10 November 2018 – Published: 22 November 2018

Abstract. The vertical profile of new particle formation (NPF) events was studied by comparing the aerosol size number distributions measured aloft and at surface level in a suburban environment in Madrid, Spain, using airborne instruments. The horizontal distribution and regional impact of the NPF events was investigated with data from three urban, urban background, and suburban stations in the Madrid metropolitan area. Intensive regional NPF episodes followed by particle growth were simultaneously recorded at three stations in and around Madrid during a field campaign in July 2016. The urban stations presented larger formation rates compared to the suburban station. Condensation and coagulation sinks followed a similar evolution at all stations, with higher values at urban stations. However, the total number concentration of particles larger than 2.5 nm was lower at the urban station and peaked around noon, when black carbon (BC) levels are at a minimum. The vertical soundings demonstrated that ultrafine particles (UFPs) are formed exclusively inside the mixed layer. As convection becomes more effective and the mixed layer grows, UFPs are detected at higher levels. The morning soundings revealed the presence of a residual layer in the upper levels in which aged particles (nucleated and grown on previous days) prevail. The particles in this layer also grow in size, with growth rates significantly smaller than those inside the mixed layer. Under conditions with strong enough convection, the soundings revealed homogeneous number size distributions and growth rates at all altitudes, which follow the same evolution at the other stations considered in this study. This indicates that UFPs are detected quasi-homogenously in an area spanning at least 17 km horizontally. The NPF events extend over the full vertical extension of the mixed layer, which can reach as high as 3000 m in the area, according to previous studies. On some days a marked decline in particle size (shrinkage)

was observed in the afternoon, associated with a change in air masses. Additionally, a few nocturnal nucleation-mode bursts were observed at the urban stations, for which further research is needed to elucidate their origin.

1 Introduction

In urban areas, traffic emissions are a major source of ultrafine particles (UFPs; Kumar et al., 2014; Ma and Birmili, 2015; Pey et al., 2008, 2009; Dall'Osto et al., 2012; Salma et al., 2014; Paasonen et al., 2016). These emissions include primary UFP exhaust emissions (Shi and Harrison, 1999; Shi et al., 2000; Charron and Harrison, 2003; Uhrner et al., 2007), the cooling of engine exhaust emissions, and the condensation of a semi-volatile-phase vapor species that creates new UFPs during dilution (Charron and Harrison, 2003; Kittelson et al., 2006; Robinson et al., 2007; Rönkkö et al., 2017). These are also considered primary particles, since they are formed near the source. Other relevant UFP sources include industrial emissions (Keuken et al., 2015; El Haddad et al., 2013), city waste incineration (Buonanno and Morawska, 2015), shipping (Kecorius et al., 2016; Johnson et al., 2014), airports (Cheung et al., 2011; Hudda et al., 2014; Keuken et al., 2015), and construction (Kumar and Morawska, 2014).

New particle formation (NPF) from gaseous precursors has been shown to cause high UFP episodes in relatively clean atmospheres due to low condensation sinks (CSs) originating from low pre-existing particle concentrations (e.g., Kulmala et al., 2000, 2004; Boy and Kulmala, 2002; Wiedensohler et al., 2002; Wehner et al., 2007; O'Dowd et al., 2010; Sellegri et al., 2010; Vakkari et al., 2011; Cusack et al., 2013a, b; Tröstl et al., 2016; Kontkanen et al., 2017). However, at mountain sites, precursors' availability seems to be the most influential parameter in NPF events, with higher values of CSs during NPF events than during non-NPF events (Boy et al., 2008; Boulon et al., 2010; García et al., 2014; Nie et al., 2014; among others). Tröstl et al. (2016) reported experimental results on nucleation driven by the oxidation of volatile organic compounds (VOCs), and Kirkby et al. (2016) reported pure biogenic nucleation.

NPF events also contribute significantly to ambient UFP concentrations in urban environments (Costabile et al., 2009; Wegner et al., 2012; von Bismarck-Osten et al., 2013, 2014; Ma and Birmili, 2015; Hofman et al., 2016; Kontkanen et al., 2017). Common features enhancing urban NPF are high insolation, low relative humidity, the availability of SO_2 and organic condensable vapors, and low condensation and coagulation sinks (Kulmala et al., 2004; Kulmala and Kerminen, 2008; Sipilä et al., 2010; Salma et al., 2016). Urban NPF episodes can be driven either regionally or locally and may or may not impact regional background areas (Dall'Osto et al., 2013; Brines et al., 2015; Salma et al., 2016). Cheung et al. (2011) and Brines et al. (2015) reported that, in urban areas, nucleation bursts without growth of particles are common, whereas the frequently occurring "banana-like" nucleation bursts at regional background sites are scarcely detected at urban sites, probably because the high CS during traffic rush hours limits the duration of the particle growth. These processes seem to prevail in summer and spring in southern European urban areas (Dall'Osto et al., 2013; Brines et al., 2014, 2015). Brines et al. (2015) also reported that, in urban environments, the highest O_3 levels occur simultaneously with NPF events, the highest SO_2 concentrations and insolation, and the lowest relative humidity and NO and NO_2 levels. This close association between O_3 and UFPs may be due to ambient conditions that favor two different, but simultaneous, processes or to the fact that they are both products of photochemical reactions in the same overall process.

Reche et al. (2011) evaluated the prevalence of primary versus newly formed UFPs in several European cities and found a different daily pattern for the southern European cities, in which the newly formed particles contributed substantially to the annual average concentrations, probably because of high insolation and possible site-specific chemical precursors. Brines et al. (2015) determined that NPF events lasting for 2 h or more occurred on 55 % of the days, and those extending to 4 h occurred on 28 % of the days, with NPF being the main contributor 14 %–19 % of the time in Mediterranean and subtropical climates (Barcelona, Madrid, Rome, Los Angeles, and Brisbane). The latter percentages reached 2 % and 24 %–28 % in Helsinki and Budapest, respectively (Wegner et al., 2012; Salma et al., 2016). Furthermore, Brines et al. (2015) calculated that 22 % of the annual average UFP number concentration recorded at an urban background site in Barcelona originated from NPF. Ma and Birmili (2015) reported that the annual contribution of traffic to the UFP number concentration was 7 %, 14 %, and 30 % at roadside, urban background, and rural sites, respectively, in and around Leipzig, Germany. On the other hand, traffic emissions contributed to 44 %–69 % of UFP concentrations in Barcelona (Pey et al., 2009; Dall'Osto et al., 2012; Brines et al., 2015), 65 % in London (Harrison et al., 2011; Beddows et al., 2015), and 69 % in Helsinki (Wegner et al., 2012).

Minguillón et al. (2015) and Querol et al. (2017) demonstrated that intensive NPF episodes take place inside the planetary boundary layer (PBL) in Barcelona, occurring around midday at surface level, when insolation and dilution of pollution are at their maxima. Earlier in the morning, NPF can only take place at upper atmospheric levels, at an altitude where pollutants are diluted, since at surface level, a high CS prevents particle formation.

While many studies have investigated NPF around the world, only a few have focused on the vertical distribution of these events (Stratmann et al., 2003; Wehner et al., 2010). In view of this, we devised a campaign with the aim to study photochemical episodes, including high O_3 levels and NPF in

the Madrid metropolitan area. In a twin article (Querol et al., 2018), the study of the temporal and spatial variability of O_3 is presented. In this work we will focus exclusively on the phenomenology of the NPF events, comparing the aerosol size distribution at surface level at urban, urban background, and suburban stations in Madrid and the outskirts of a residential village 17 km from Madrid. We also study the vertical distribution of the events using airborne instrumentation carried by tethered balloons.

2 Methodology

2.1 The study area

The Madrid metropolitan area (MMA) lies in the center of the Iberian Peninsula at an elevation of 667 m a.s.l. (meters above sea level). It is surrounded by mountain ranges and river basins that channel the winds in a NE–SW direction. Having an inland Mediterranean climate, winters are cool and summers are hot, and precipitation occurs mainly in autumn and spring. Road traffic and residential heating in winter are the main sources of air pollutants, with small contributions made by industrial and aircraft emissions (Salvador et al., 2015).

In summer, the area is characterized by strong convection, which results in PBL heights as high as 3000 m a.g.l. (above ground level) and mesoscale recirculation caused by anabatic and katabatic winds in the surrounding mountain ranges (Plaza et al., 1997; Crespí et al., 1995), which can lead to the accumulation of pollutants if the recirculation persists for several days.

The cold and warm advection of air masses associated with the passage of upper-level troughs and ridges over the area gives rise to a sequence of accumulation and venting periods, respectively. During accumulation periods, pollutants accumulate in the area, and concentrations increase for 2–6 days, until a trough aloft brings a cold advection and a venting period starts. For a detailed description of the meteorological context during the campaign, see Querol et al. (2018).

A few studies have focused on NPF events in the area. For instance, Gómez-Moreno et al. (2011) reported NPF episodes in Madrid to be "not a frequent phenomenon", since only 63 events per year were detected, with 17 % of the total days occurring mostly in spring and summer. However, Brines et al. (2015) reported both intensive summer and winter NPF episodes at the same station, which accounted for 58 % of the time as an annual average, considering the prevalence of nucleation bursts for 2 h or more. Alonso-Blanco et al. (2017) described the phenomenology of particle-shrinking events, i.e., a decline in particle size caused by particle-to-gas conversion, at an urban background station in Madrid (CIEMAT), stating that they occur mainly between May and August in the afternoon, due to either a change in wind direction or the reduction of photochemical processes. Particle shrinkage following their growth is not a common phenomenon but has been observed in a few areas around the world. Yao et al. (2010), Cusack et al. (2013a, b), Young et al. (2013), Skrabalova et al. (2015), and Alonso-Blanco et al. (2017) and references therein, reported shrinkage rates ranging from -1.0 to $-11.1\,\mathrm{nm\,h^{-1}}$.

2.2 Instrumentation

The data used in this study were collected during a summer campaign in and around Madrid in July 2016. Three air quality supersites were used, namely, an urban station, an urban background station, and a suburban station, in addition to a setting in a suburban environment with two tethered balloons that allowed for the study of the vertical distribution of aerosols and air pollutants. All stations are located within a range of 17 km. A map displaying all locations is shown in Fig. 1.

The CSIC (Consejo Superior de Investigaciones Científicas, the Spanish national research council) urban station, operative from 9 to 20 July, was located in the Institute of Agricultural Sciences (40°26′25″ N, 03°41′17″ W, 713 m a.s.l.) in central Madrid. The instrumentation at this station was installed on the sixth floor of the building, with instruments sampling through a window. NO_x and equivalent black carbon (BC) concentrations were measured with a chemiluminescence-based analyzer (Teledyne API, 200EU) and an Aethalometer (AE33, Magee Scientific, $5\,\mathrm{L\,min^{-1}}$), respectively. The aerosol number size distribution in the size range 8–120 nm was measured with a Scanning Mobility Particle Spectrometer (SMPS; TSI, 3082) equipped with a Nano-Differential Mobility Analyzer (DMA; TSI 3085) and a condensation particle counter (CPC; TSI 3772, $1\,\mathrm{L\,min^{-1}}$). A particle size magnifier (PSM, Airmodus A10) combined with a CPC (TSI 3775) were used to measure size distributions in the size range 1.2–2.5 nm. This system was operated in scanning mode using Airmodus software ($2.5\,\mathrm{L\,min^{-1}}$). PSM data were post-processed and corrected for diffusion losses by using tailored software provided by Airmodus.

The CIEMAT (Centro de Investigaciones Energéticas, Medioambientales y Tecnológicas, Research center for energy, environment, and technology) urban background station, operative from 4 to 20 July, was located on the outskirts of Madrid, 4 km from the CSIC station (40°27′23″ N, 03°43′32″ W, 669 m a.s.l.). NO_x, O_3, and BC concentrations were measured with a chemiluminescence-based analyzer (THERMO 17i), an ultraviolet photometry analyzer (THERMO 49i), and an Aethalometer (AE33 Magee Scientific, $5\,\mathrm{L\,min^{-1}}$), respectively. The aerosol number size distribution in the size range 15–660 nm was measured with an SMPS (TSI 3080) combined with a CPC (TSI 3775, $1.5\,\mathrm{L\,min^{-1}}$) and in the size range 1–30 nm was measured with a 1 nm SMPS (TSI 3938E77, $2.5\,\mathrm{L\,min^{-1}}$). All data were processed and corrected for multiple charge and diffusion losses by using the TSI Aerosol Instrument Manager

Figure 1. Location of the stations and sounding setting used in the campaign. The location of the airport is also shown. A white solid line marks the city limits of Madrid.

(AIM) software. In the overlapping range (15–30 nm), the nano-SMPS yielded slightly higher concentration values. In order to correct these higher values and obtain a continuous size distribution, the daily nano-SMPS values were corrected to adapt to those of the SMPS. We compared the resulting merged particle size distribution with CPC measurements (CPC TSI 3776, > 2.5 nm) to check that there was good agreement in total particle concentration. Temperature (4 m a.g.l.), relative humidity (4 m a.g.l.), solar radiation (35 m a.g.l.), and wind speed and direction (55 m a.g.l.) were measured at a meteorological tower at the station.

The ISCIII (Instituto de Salud Carlos III, Carlos III Institute of Health) suburban station was located at the Carlos III Institute of Health in Majadahonda, 15 km from the CSIC station (40°27′27″ N, 03°51′54″ W, 739 m a.s.l.), and was operative from 4 to 20 July. An SMPS (TSI 3080) equipped with a CPC (TSI 3775, 1.5 L min^{-1}) measured the aerosol number size distribution in the size range 9–360 nm. Data were processed and corrected for multiple charge and diffusion losses by using the TSI AIM software. Size distributions in the range 1.2–4.0 nm were measured with a PSM (Airmodus, A11, 2.5 L min^{-1}) in combination with a CPC (Airmodus, A20) working in scanning mode. Data were post-processed and corrected for diffusion losses by using the Scilab code provided by Airmodus. A proton-transfer-reaction time-of-flight mass spectrometer (PTR-ToF-MS; Ionicon Analytik, PTR-TOF 8000) operating in H3O+ mode was used to measure VOC concentrations. A detailed description of the instrument can be found in Graus et al. (2010). The operational procedure for the PTR-ToF-MS is fully described in Querol et al. (2018). Results regarding these measurements are briefly presented in Sect. S1 in the Supplement.

UFP instrument calibration was performed by the manufacturers: TSI in the case of SMPS and CPCs and Airmodus for PSM. Particle sizing and counting instrumentation at all stations were collocated next to windows or walls where holes were available for inlets and equipped with individual 1/4 inch, 20 cm long conductive silicone tubing inlets for PSM. SMPS and CPC also had individual 30 cm conductive silicone tubing inlets. Each instrument had its own flow rate since there were individual inlets. TSI instrument data were corrected for diffusion losses and multiple charge losses using the instruments' own software.

Regarding the vertical measurements, two tethered balloons carrying miniaturized instrumentation were based at the Majadahonda (MJDH) rugby field (40°28′29.9″ N 3°52′54.6″ W, 728 m a.s.l.), 17 km from CSIC. Twenty-eight flights up to 1200 m a.g.l. were carried out from 11 to 14 July. A miniaturized SMPS (Hy-SMPS, an SMPS designed by the University of Hanyang) measured the particle size distribution in the range 8–245 nm with a time resolution of 45 s and flow of 0.125 L min^{-1} (Lee et al., 2015). However, only particles larger than 10 nm could be detected due to lower efficiency for finer particles. The instrument was inter-compared with an SMPS (TSI, Standard DMA with 3776 CPC) for 50 nm monodispersed NaCl particles and polydispersed aerosols (Fig. S1). The number concentration of particles larger than 3 nm was measured with a miniaturized butanol-based CPC (Hy-CPC, designed by the University of Hanyang). The time resolution was 1 s, and sample flow was 0.125 L min^{-1} (Lee et al., 2014). Temperature, relative humidity, pressure, wind speed, and wind direction were also measured. The instrumentation was also equipped with a global positioning system (GPS). An additional set of miniaturized instrumentation was placed at surface level for comparison.

2.3 Data analysis techniques

Identification of NPF events was made via the method proposed by Dal Maso et al. (2005). After the examination of the daily particle size distribution, if the day was classified as an event day, we proceeded to calculate growth rates (GRs), shrinking rates (SRs), condensation and coagulation sinks (CSs and CoagSs), and formation rates (J_{D_p}).

The algorithm proposed by Hussein et al. (2005) was used to fit log-normal modes to the particle size distribution, from which GRs were calculated by following Eq. (1):

$$\mathrm{GR} = \frac{\mathrm{d}D_\mathrm{p}}{\mathrm{d}t}, \quad (1)$$

where D_p is the selected geometric mean diameter corresponding to the growing particle mode. Unless stated otherwise, in this work, GRs are calculated for particles growing from 9 to 25 nm. When calculating GRs with PSM data, the

range was selected according to the measuring range of each instrument (see Sect. 2.2). SRs were calculated analogously when a decrease in the diameter of the fitted modes was observed.

The CS, a measure of the removal rate of condensable vapor molecules due to their condensation onto pre-existing particles (Kulmala et al., 2012), is calculated using Eq. (2):

$$\mathrm{CS} = 2\pi D \sum_i \beta_i D_{\mathrm{p},i} N_i, \tag{2}$$

where D is the diffusion coefficient of the condensing vapor (here we use H_2SO_4), $D_{\mathrm{p},i}$ and N_i are the particle diameter and particle concentration, respectively, for the size class i, and β_i is the transitional correction factor:

$$\beta_i = \frac{1 + K_i}{1 + \left(\frac{4}{3\alpha} + 0.337\right) K_i + \frac{4}{3\alpha} K_i^2}, \tag{3}$$

where the Knudsen number $K_i = 2\lambda / D_{\mathrm{p},i}$, with λ representing the mean free path of the condensing vapor in air and α representing the sticking coefficient, here assumed to be equal to 1.

The formation rates of particles were calculated as 30 min averages, following Eq. (4):

$$J_{D_\mathrm{p}} = \frac{\mathrm{d}N_{D_\mathrm{p}}}{\mathrm{d}t} + \mathrm{CoagS}_{D_\mathrm{p}} \cdot N_{D_\mathrm{p}} + \frac{\mathrm{GR}}{\Delta D_\mathrm{p}} N_{D_\mathrm{p}}, \tag{4}$$

where we use the PSM measuring range for N_{D_p}, and CoagS is a quantification of the ability of the preexisting aerosols to scavenge newly formed particles. For its calculation we take the geometric mean diameter of the size ranges 1–25 nm, using a merged PSM and SMPS particle size distribution. The CoagS can be calculated using Eq. (5):

$$\mathrm{CoagS}_{D_\mathrm{p}} = \sum_{D'_\mathrm{p}} K\left(D_\mathrm{p}, D'_\mathrm{p}\right) N_{D'_\mathrm{p}}, \tag{5}$$

where K is the coagulation coefficient. For a detailed description of the parameters and their derivation, see Kulmala et al. (2012).

A rough estimation of the mixed layer height was determined using Hy-CPC measurements. The top of the mixed layer was considered to be at an altitude at which particle concentration decreases an order of magnitude quasi-instantaneously and remains constant above this altitude. All UFP profiles are included in Querol et al. (2018).

Additionally, bivariate polar plots of concentration have been used to relate wind speed and direction with total particle concentration using PSM data by means of the R package "openair" (Carslaw and Ropkins, 2012).

3 Results and discussion

3.1 Meteorological context

Figure S2 shows the evolution of the temperature, relative humidity, wind speed, and wind direction measured at CIEMAT from 5 to 20 July 2016. The evolution of temperatures during this period evidences a succession of accumulation and venting episodes. Rain gauges collected significant precipitation only on 6 July at midnight (not shown).

The balloon field campaign, held from 11 to 14 July, coincided with the start of a venting period, the passage of an upper-level trough, and the transition to an accumulation period when the trough moved to the east of the Iberian Peninsula and a ridge passed over the area of study (see Fig. S3). Maxima and minima temperatures dropped, while strong westerly winds predominated until they veered to the NE on 12 July 18:00 UTC. High nocturnal wind speed peaks were recorded in this period and were often accompanied by a change in wind direction. For detailed information on the meteorological parameters during this campaign, see Querol et al. (2018).

3.2 Comparison of NPF events at urban and suburban surface stations

In the following discussions, we group CSIC (urban) and CIEMAT (urban background) as urban stations and compare them to ISCIII (suburban). This grouping is done because of the availability of data during the period of interest. However, it has to be noted that CSIC is more influenced by traffic than CIEMAT, therefore it is more representative of urban environments, and, for this reason, CSIC data are chosen when possible. Eighteen NPF episodes have been identified on a total of 7 days throughout the campaign. A summary of these events is presented in Table 1. Out of these, a total of 14 events on 6 days had simultaneous data available for at least one of the urban stations (CSIC, CIEMAT) and the suburban station (ISCIII). These episodes, marked with an asterisk in Table 1, are selected for further analysis in this section. Figure 2 represents the aerosol number particle size distributions for the selected episodes (12–18 July 2016).

3.2.1 Episode characteristics

In the selected episodes, intensive daytime nucleation and subsequent condensational growth processes took place simultaneously at urban and suburban stations, located 17 km apart, and, accordingly, we classify these as regional NPF episodes. If the episodes were caused by primary emissions, then we would observe different size distributions at all stations, because each one of them is differently influenced by traffic. The urban station is largely influenced by traffic emissions, whereas the suburban station is much less affected by these emissions. Since we observe the same size distribution at both stations, we can say that traffic emissions are not the

Table 1. Summary of new particle formation events recorded during the campaign, showing the starting time, considered as the moment of first detection of the nucleation mode, the final time, considered as the time when the mode reaches 25 nm, the growth rate calculated in that period using SMPS and PSM data, and formation rates at the starting time. An asterisk marks the events that are detected simultaneously at all stations and were chosen for further analysis in this work.

	Date (dd/mm/yyyy)	Starting time (UTC)	Final time (UTC)	GR ($nm\,h^{-1}$)	GR_{PSM} ($nm\,h^{-1}$)	J_1 ($cm^{-3}\,s^{-1}$)
CSIC	12/07/2016 (*)	06:20	10:39	3.9	1.9	2.4
	13/07/2016 (*)	08:30	12:49	2.0	1.1	8.5
	14/07/2016 (*)	08:45	11:53	1.4	6.75	15.7
ISCIII	12/07/2016 (*)	05:30	09:44	3.0	0.7	1.9
	13/07/2016 (*)	08:50	11:54	4.6	4.3	8.1
	14/07/2016 (*)	09:20	10:39	7.6	6.8	6.5
	16/07/2016 (*)	–	–	–	4.3	–
	17/07/2016 (*)	–	–	–	4.4	3.2
	18/07/2016 (*)	10:44	12:20	2.9	1.38	6.8
CIEMAT	13/07/2016 (*)	08:15	13:45	2.5	–	–
	14/07/2016 (*)	09:00	13:10	4.1	–	–
	15/07/2016	08:34	13:08	4.0	–	–
	18/07/2016 (*)	09:09	11:49	2.6	–	–
MJDH Sounding	12/07/2016	07:27	08:08	3.5	–	–
	13/07/2016	08:39	09:56	5.3	–	–
	14/07/2016	09:00	10:34	6.2	–	–

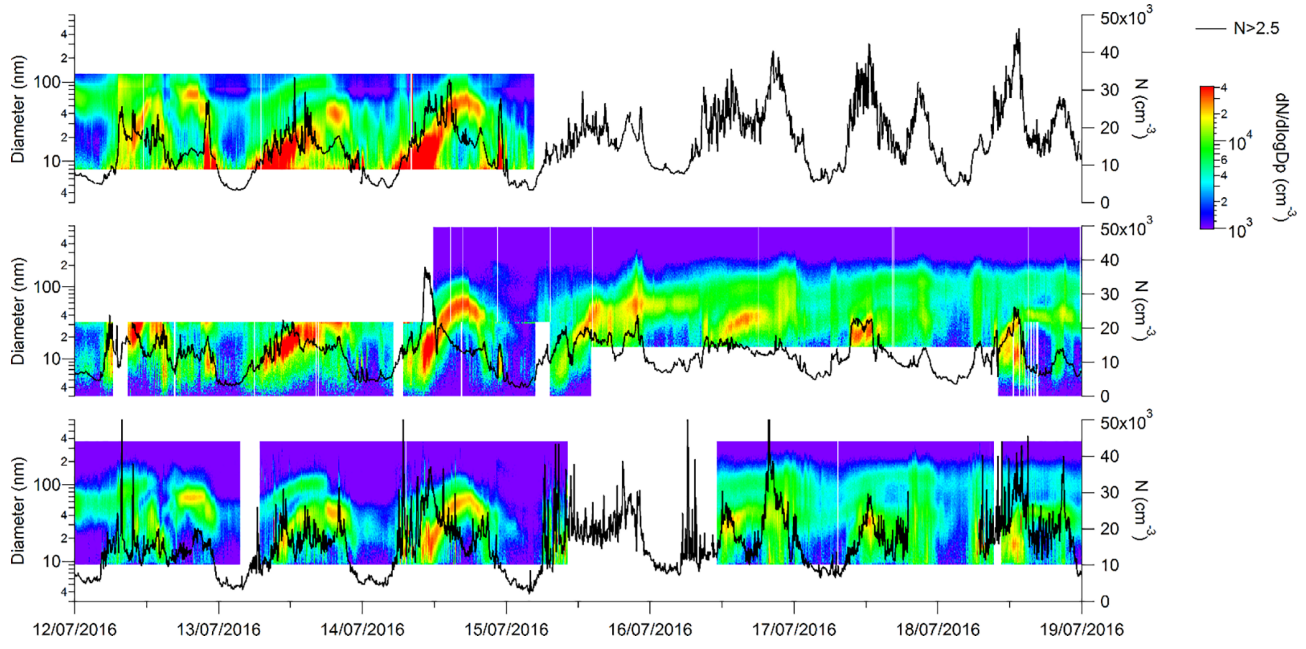

Figure 2. Particle size distribution at CSIC, CIEMAT, and ISCIII (top to bottom), from 4 to 20 July 2016. Total particle concentration of particles with diameter greater than 2.5 nm is also shown.

origin of the observed distributions. Additional arguments include the fact that number concentrations of sub-25 nm particles peak at noon, when BC levels are at their minimum, as well as the concentration of particles measured by PSM being higher at the suburban station compared to the urban station, implying that the particles did not originate from traffic sources.

At urban stations, particles of the order of 10 nm are detected throughout the day, even during the night. Conversely, at the suburban station, such small particles are only detected

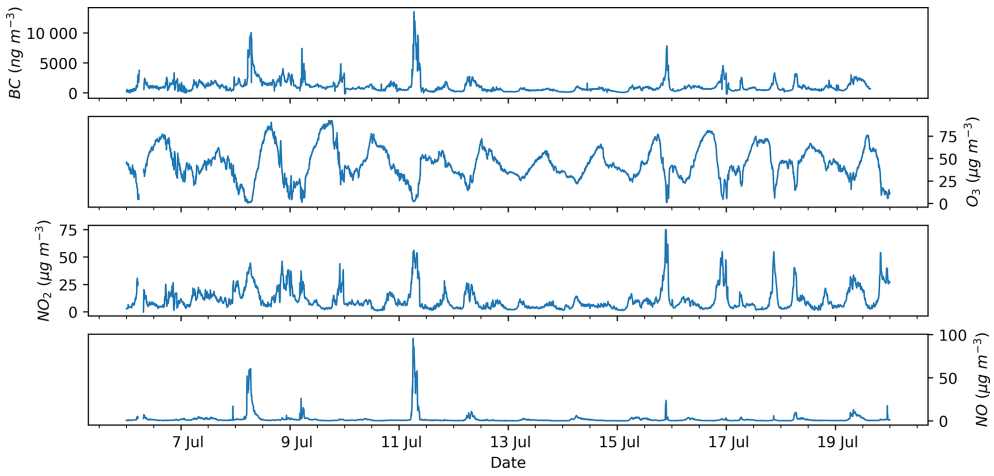

Figure 3. Concentrations of BC, O_3, NO, and NO_2 measured from 6 to 20 July 2016 at CIEMAT.

during daytime. Additionally, during some days, a very intense short nucleation burst is registered at around midnight local time at urban stations, but nothing of this nature is detected at the suburban station. This phenomenon is analyzed in Sect. 3.4.2.

Despite the detection of sub-10 nm particles as early as 04:00 UTC (06:00 LT – local time) at the urban stations, only after around 09:00 UTC is the growth of the particles observed, occurring roughly at the same time in both urban and suburban stations. Newly formed particles grow until they have reached sizes of up to 50 nm, usually around 13:00 UTC (15:00 LT). After this, shrinkage is observed on 10 days, corresponding to 71 % of the days with available data. Consequently, the evolution of the particle size distribution is arc-shaped in these cases.

It should be noted that nucleation episodes coincide in time with the early increases in O_3 concentrations in the morning, whereas the occurrence of maximum O_3 concentration (120 to 150 $\mu g\,m^{-3}$ hourly daily maxima between 14:00 and 16:00 UTC; see Fig. 3) takes place during the UFP growth stage, since oxidation of VOCs and inorganic gases is also accelerated with photochemistry and the presence of O_3 and OH radicals, among others (Coleman et al., 2008; Wang et al., 2017; Saiz-Lopez et al., 2017).

3.2.2 Comparison of GR, J_1, CS, and CoagS

For the observed daily regional NPF events, GRs for the nucleation mode, J_1, CSs, and CoagSs have been determined using PSM and SMPS aerosol size distribution measurements. Here, the GR is calculated from the time of detection of the smallest mode until either the particle reaches 25 nm or it stops growing before reaching that size. We considered only the events that are observed simultaneously at the suburban station and at least at one urban station (highlighted in Table 1). GRs regarding the vertical measurements are discussed in the following section due to differing sampling periods.

The calculated GR for the surface stations are shown in Table 1. GRs ranged from 2.9 to 7.6 $nm\,h^{-1}$ at the suburban site, with a mean value of $4.5 \pm 2.1\,nm\,h^{-1}$, and from 1.4 to 4.0 $nm\,h^{-1}$ at the urban stations, with a mean value of $2.8 \pm 1.0\,nm\,h^{-1}$. We cannot affirm that the mean value of the suburban station is higher than that of the urban stations, because the mean value of the GR at urban stations is included in the confidence interval of the GR at the suburban station. It also has to be considered that only 7 days of measurements are available for these calculations, hence further studies would be needed to confirm the observed differences between urban and suburban stations. Nevertheless, the GRs calculated are consistent with those observed by Alonso-Blanco et al. (2017), ranging 1.4–10.6 $nm\,h^{-1}$ at CIEMAT.

The GRs calculated in this study are also consistent with those observed in other urban and suburban areas. Kulmala et al. (2004) concluded that typical GRs are 1–20 $nm\,h^{-1}$ in midlatitudes. In particular, Stolzenburg et al. (2005) observed GRs ranging from 2.4 to 8.5 $nm\,h^{-1}$ in regional events in an urban environment in Atlanta, GA, US. Qian et al. (2007) reported regional events with a median GR of 5.1 $nm\,h^{-1}$ in an urban environment in St. Louis, MO, US. Ahlm et al. (2012) reported an average GR of 7.3 $nm\,h^{-1}$ in Bakersfield, CA, US. Manninen et al. (2010) characterized NPF events at 12 European sites. Cabauw (the Netherlands) and San Pietro Capofiume (Italy) are stations located in environments comparable to that in our suburban station, ISCIII. For these stations, the observed median GRs were 7–8 $nm\,h^{-1}$, corresponding well with our calculated GR for the suburban station.

Figure 4 shows the average daily cycles of particle concentrations in the size ranges 9–25 nm ($N_{9–25}$) and 1.2–2.5 nm ($N_{1.2–2.5}$), where the total particle concentration was measured by the PSM ($N_{>2.5}$), CS, and CoagS during the re-

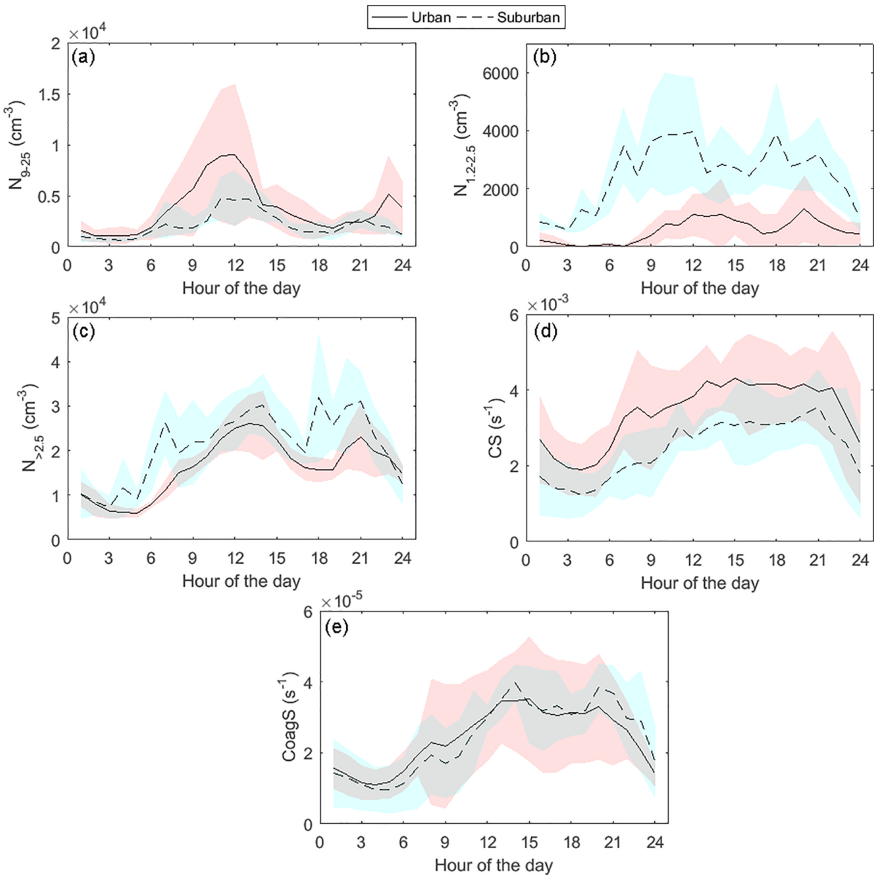

Figure 4. Mean daily cycles of **(a)** total particle concentration in the size range 9–25 nm, **(b)** total particle concentration in the size range 1.2–2.5 nm measured with PSM at CSIC and ISCIII, **(c)** total concentration of particles > 2.5 nm measured with PSM at CSIC and ISCIII, **(d)** condensation sink (CS), and **(e)** coagulation sink (CoagS) during regional new particle formation events at urban (CSIC and CIEMAT, solid line) and suburban (ISCIII, dashed line) stations. Red (urban) and blue (suburban) shaded shapes show 95 % confidence intervals. The hour of the day is given in UTC. Local time is UTC + 2 h.

gional NPF events at the urban and suburban stations. Average $N_{9–25}$ daily mean values are 3.7×10^3 and 2.2×10^3 cm^{-3} at the urban and suburban stations, respectively. $N_{>2.5}$ has average daily mean values of 1.6×10^4 and 2.1×10^4 cm^{-3} at the urban and suburban stations, respectively. It has to be highlighted that $N_{1.2–2.5}$ is considerably larger at the suburban station throughout the day, with mean values of 2.5×10^3 cm^{-3}, compared to 0.5×10^3 cm^{-3} at the urban stations. CSs and CoagSs have average daily mean values of 3.4×10^{-3} s^{-1} (2.5×10^{-3} s^{-1} at the suburban station) and 2.4×10^{-5} s^{-1}, respectively. After dawn, anthropogenic activities start, and $N_{9–25}$, $N_{1.2–2.5}$, $N_{>2.5}$, CSs, and CoagSs start to increase at the same time, both in the urban and suburban environments. Around 07:00 UTC, once the morning traffic rush diminishes, $N_{9–25}$, $N_{>2.5}$ and the sinks increase more slowly; moreover, total particle concentration decreases in the suburban station, indicating that, in this environment, the impact of the traffic emissions on total particle concentration is smaller than near the city center, as expected. Shortly afterwards, at 09:00 UTC, the photochemical processes are strong enough to start NPF, as suggested by the increase in particle concentrations, while the sinks achieve relative minimums. $N_{9–25}$ reaches its maximum at midday (9×10^3 and 5×10^3 cm^{-3} at the urban and suburban stations, respectively) and then decreases because the particles start growing to diameters greater than 25 nm, adding to the sinks, which increase gradually until the evening. NPF leads to maximal UFP concentrations around midday at all stations, as suggested by the peak in $N_{>2.5}$, which is recorded simultaneously with very low BC levels (see Figs. 3 and S4). Around 19:00 UTC, the effect of the afternoon traffic rush is evident, as the variables evolve in a manner similar to that in the morning. Finally, at 23:00 UTC, a sharp and short increase in $N_{9–25}$ is observed, associated with the aircraft emissions discussed in Sect. 3.4.2.

Growth rates (GR_{PSM}) and total formation rates of 1.2–4.0 nm particles (J_1) were calculated from PSM data at CSIC and ISCIII stations. GR_{PSM} were calculated from 11 to 18 July 2016, averaging 4.3 nm h^{-1} at the urban station and 3.7 nm h^{-1} at the suburban station. J_1 were calculated only

for the days in which NPF is identified. The results for these days are included in Table 1. Average J_1 values are higher at the urban station ($8.9\,cm^{-3}\,s^{-1}$) compared to the suburban station ($5.3\,cm^{-3}\,s^{-1}$). Concentrations of 1.2–4.0 nm particles are lower at the urban station (Fig. S4), which could lead to lower formation rates. However, the coagulation sink is greater at the urban station, as discussed before, which contributes to the second factor in Eq. (4). It has to be noted that only 3 days of overlapping between PSM and SMPS data were available for NPF events at the urban station and 6 days at the suburban station. A larger dataset would be needed to confirm these results.

The average values of the formation rates agree with those reported at similar stations around the world. For instance, Woo et al. (2001) reported J_3 ranging from 10 to $15\,cm^{-3}\,s^{-1}$ in Atlanta, GA, US. Wehner and Wiedensohler (2003) reported an average J_3 of $13\,cm^{-3}\,s^{-1}$ in Leipzig, Germany. Hussein et al. (2008) reported nucleation rates ($D_p < 25$ nm) ranging from 2.1 to $3.0\,cm^{-3}\,s^{-1}$ in summer in Helsinki, Finland.

3.3 Vertical distribution of NPF events

3.3.1 UFP concentrations

Querol et al. (2018) studied the vertical profiles of UFP and O_3 concentrations measured during the campaign using the balloon soundings at Majadahonda. UFP concentrations are homogeneous throughout the mixing layer and present a sharp decrease at the top. As the day progresses, convection is more effective, and high UFP levels reach higher altitudes as the mixing layer heightens. Moreover, the concentrations tend to increase until midday. Afterwards, they remain constant or decrease slightly, always showing homogeneous levels from surface levels to the top of the PBL. Concentrations of UFPs increased markedly from 11 to 14 July, both at the surface and upper levels. This is consistent with the observed decrease in the convective activity during that period, evidenced by a decrease in temperatures, but also with an increase in the formation rates calculated in this study. Therefore, the increase in particle concentration is probably the result of both a decline in PBL height and more intense nucleation episodes.

3.3.2 Particle size distribution and NPF episodes

The NPF events described in Sect. 3.2 that took place between 12 and 14 July were not only detected at surface level, but also in the upper layers with the balloons soundings in Majadahonda. However, the measurements were not continuous, since the balloons could not be operated safely if the wind speed was above $8\,m\,s^{-1}$ at any vertical level.

Figure 5 shows the fitted modes to the particle size distribution measured in the soundings on 12 July. The fact that sub-40 nm particles are not detected at the higher levels of the first flights suggests that convection is not very effective yet, and the sounding goes through different atmospheric layers, most likely the mixed layer and the residual layer. In the residual layer, Aitken-mode particles formed on previous days prevail (Stull, 1988). The interphase between the mixed layer and the residual layer, i.e., the mixed layer height, has been derived using the UFP vertical profiles (see Querol et al., 2018). From 10:00 UTC onwards, once convection has fully developed, the mixed layer covers all the sounding, and we see a homogeneous distribution at all levels, which is also comparable to those recorded with the instrumentation measuring at the surface. This agrees with the fact that UFPs are homogeneously distributed in the mixed layer and are detected at higher altitudes as the mixed layer rises.

In the early morning the size distribution is dominated by a 60 nm mode at all altitudes, which grows to 100 nm at 11:00 UTC. Even though it is detected at all levels, the mode decreases slightly in size when the sounding ascends above the mixed layer limit, which is more clearly visible on the second flight at around 09:00 UTC. This result suggests that there are lower vapor concentrations in the residual layer, which inhibits particle growth, whereas the mixed layer is more polluted, spurring faster particle growth. The GRs calculated for this mode were $1.8\,nm\,h^{-1}$ in the residual layer and $7.3\,nm\,h^{-1}$ in the mixed layer. The concentration and size of the Aitken mode decrease after midday, which might be related to an increase in wind speed, entailing dilution and evaporation; this leads to the shrinking of the particles. Because of the increase in wind speed, the balloons could not be operated safely, and no additional flights were made on that day.

Moreover, during the morning, we observed particles growing inside the mixing layer, from 10 nm at 07:00 UTC to 30 nm at midday. This mode is observed simultaneously at ISCIII; therefore, we consider it for calculation. The GR obtained is $3.5\,nm\,h^{-1}$. The fact that the GR is the same throughout the mixing layer, even though we expect VOCs to be higher near the surface, upholds the assumption that the convection is very efficient and the entire layer is well-mixed. After 13:00 UTC, due to the increase in wind speed, particles start to shrink. While concentrations were not as high as they were during other episodes, the evolution is remarkably similar to the NPF event measured at the same time at ISCIII, which had a GR of $3.0\,nm\,h^{-1}$.

The size distribution and the corresponding fitted modes for the soundings made on 13 July are presented in Fig. 6. Although the balloons could not fly until 10:30 UTC for safety reasons, at least two modes are detected from early morning at the sounding location. A mode starting roughly at 40 nm at 07:00 UTC grows to 100 nm at 15:00 UTC. With a GR of $8.5\,nm\,h^{-1}$, this mode was detected at all altitudes once the soundings started, indicating that the convection was already effective by 10:30 UTC and all the measured altitudes were completely mixed, leading to a homogeneous particle distribution throughout the soundings. This mode is the prolon-

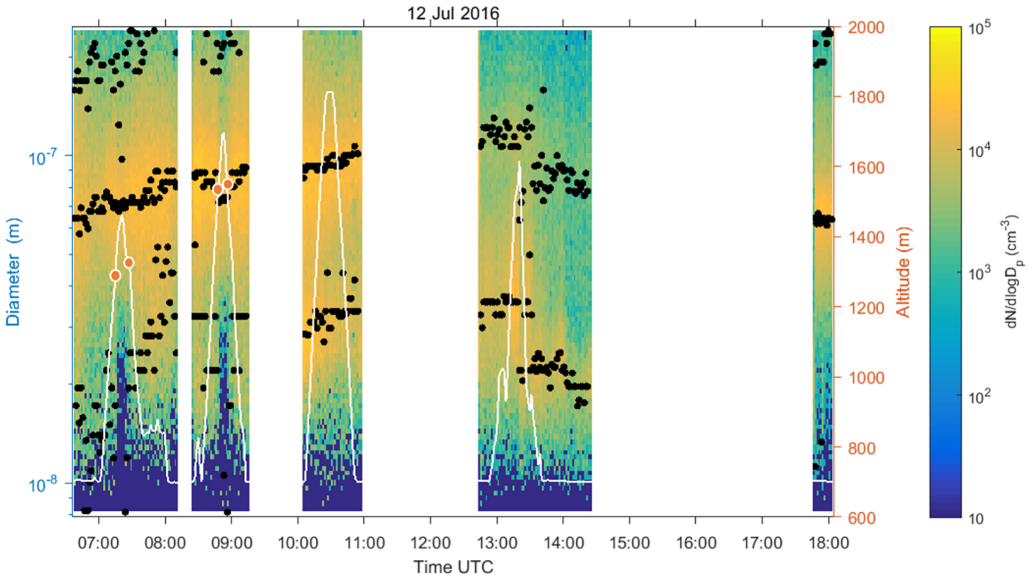

Figure 5. Particle size distribution with fitted log-normal modes (black dots) measured during the balloon soundings at Majadahonda on 12 July 2016. An estimation of the mixing layer height is represented with orange dots. The altitude of the instrumentation is represented with a white line. Surface level is 630 m above sea level. Time is UTC. Local time is UTC + 2 h.

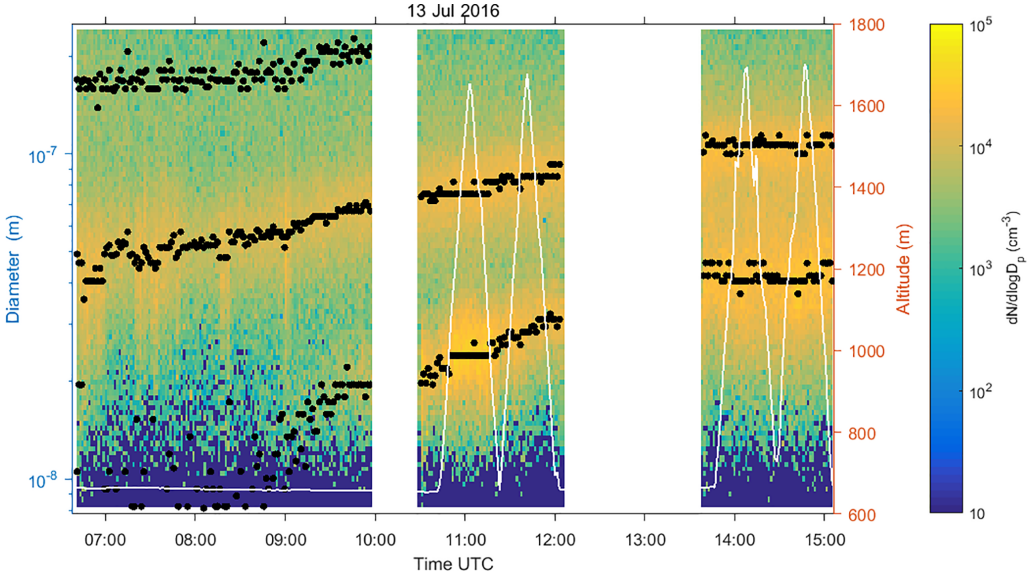

Figure 6. Particle size distribution with fitted log-normal modes (black dots) measured during the balloon soundings at Majadahonda on 13 July 2016. The altitude of the instrumentation is represented with a white line. Surface level is 630 m a.s.l. Time is UTC. Local time is UTC + 2 h.

gation of the Aitken mode detected the day before, which shrank from midday until the following morning. It is also detected at ISCIII and CSIC, with GRs of 7.5 and 6.9 nm h^{-1}, respectively. A nucleation mode also grew from the detection limit of the instrument, from around 10 nm at 08:30 UTC to 40 nm at 15:00 UTC. Comparing with other stations, we considered this mode only after 09:00 UTC and calculated the GR from that time. We consider this a regional NPF event, since the start of the particle growth is registered simultaneously at all the stations. The GRs at the sounding location, ISCIII and CSIC are 5.3, 4.6, and 2.0 nm h^{-1}, respectively.

Figure 7 shows the particle size distribution and fitted modes for the soundings made on 14 July. Correspondingly, in Fig. 8, the vertical distribution of particles for some of the soundings is presented. The earliest soundings revealed the existence of a residual layer aloft. In order to verify this

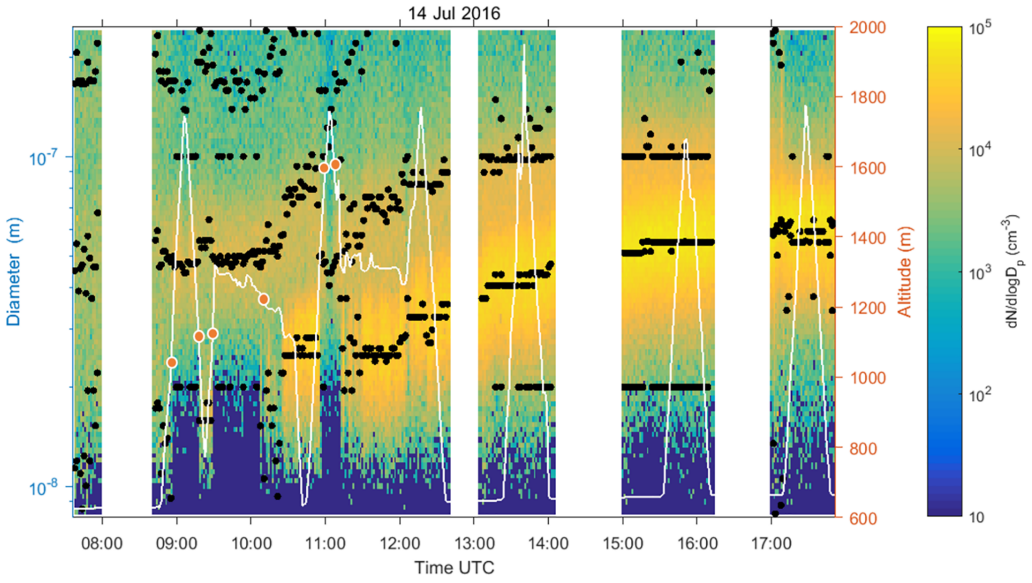

Figure 7. Particle size distribution with fitted log-normal modes (black dots) measured during the balloon soundings at Majadahonda on 14 July 2016. The altitude of the instrumentation is represented with a white line. An estimation of the mixing layer height is represented with orange dots. Surface level is 630 m above sea level. Time is UTC. Local time is UTC + 2 h.

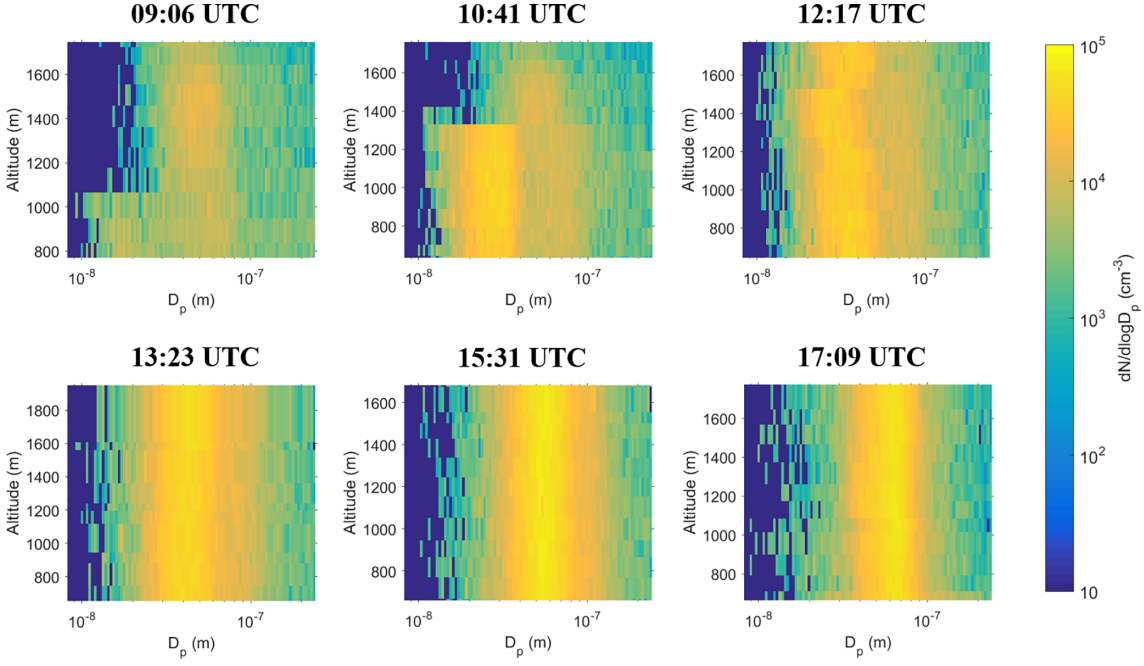

Figure 8. Vertical particle size distribution measured on 14 July during selected soundings.

result, two constant altitude flights were made during the morning. The extension of the wire was not modified during these flights. However, changing wind conditions varied the altitude of the instruments slightly. The altitude was chosen so that the instruments initially remained outside the mixing layer, i.e., inside the residual layer. As the insolation increased, so did the altitude of the mixing layer, until it reached the altitude at which the balloons were positioned. As the mixing layer reached the balloons, total particle concentration increased sharply from 4×10^3 to 2×10^4 cm^{-3}, demonstrating that newly formed particles remain inside the mixing layer.

According to the abrupt decline in particle concentration, the boundary between the mixing and residual layers was lo-

cated at 1000 m at 09:00 UTC, 1200 m at 10:00 UTC, 1350 m at 11:00 UTC, and beyond 1800 m after 12:00 UTC. This can be taken as an indicator of the effectiveness of convection, meaning that after 12:00 UTC, the whole measured particle population was well mixed throughout the sounding range. Inside the residual layer, particles had a slower GR ($0.5\,nm\,h^{-1}$ compared to $8.45\,nm\,h^{-1}$ for the 40 nm mode – note that due to the use of a log scale, this might be unnoticeable visually), and no particles smaller than 20 nm were observed.

Nucleation mode particles were detected exclusively inside the mixing layer from 08:00 to 12:00 UTC, whereas growth was only observed from 09:00 to 11:00 UTC and from 12:00 UTC onwards. The time spacing between both growth periods coincides with a marked decrease in wind speed. During the first period, GRs at the sounding station, ISCIII, and CSIC were 6.2, 5.4, and $1.4\,nm\,h^{-1}$, respectively. However, during the second stage, particles grew faster at the urban station ($8.6\,nm\,h^{-1}$) than at the sounding location ($4.5\,nm\,h^{-1}$). As the latter is a suburban environment, this contrasts with the results obtained in Sect. 3.2.2. This fact could be explained by the veer of NE winds to weaker southerly winds in Madrid, which was not observed in Majadahonda.

Overall, the soundings revealed that there is simultaneous growth and shrinking of nucleation and Aitken modes and that both of them grow and shrink at different rates. This was also observed in the surface measurements when comparing urban and suburban stations (see Sect. 3.2.2).

3.4 Other observations

3.4.1 Prevalence of particles and shrinkage

A further interesting feature is the presence of the Aitken mode on most days. Usually in the size range between 50–100 nm, reaching 110 nm in some cases, this mode does not correspond to newly formed particles, but it follows a parallel evolution (condensational growth and potential shrinkage). When looking at the evolution of aerosol size distributions on consecutive days, it is possible to see a connection between this 50–100 nm mode and the distribution of the previous days. The nucleated and grown mode from one day is still present the following day, and it continues to grow until it eventually fades away or grows beyond the detection limits of the instruments. On some occasions, the Aitken mode can be tracked for 2 or more consecutive days, alternating between the stages of growth and shrinkage.

The start of the shrinking phase coincides with a marked increase in wind speed (Fig. S5); therefore, it is associated with dilution, which favors the evaporation of semi-volatile vapors, resulting in a decline in particle diameter and concentrations, as observed in most cases. The calculated shrinkage rates are shown in Table S1. SRs for particles with a starting diameter below 40 nm range from -1.1 to $-8.0\,nm\,h^{-1}$. For particles in the Aitken mode above 40 nm, the values fall between -4.9 and $-20.5\,nm\,h^{-1}$. The results seem to indicate that, the larger the starting diameter, the faster the particles shrink. Since shrinkage is observed simultaneously at urban and suburban stations, shrinkage seems to be a regional phenomenon in the Madrid area, as already suggested by Alonso-Blanco et al. (2017). However, we could only identify a limited number of simultaneous shrinking episodes, and further research would be needed to confirm these results.

3.4.2 Nocturnal UFP peaks

Although outside of the major focus of this study (photochemical nucleation), other interesting events were detected which took place at night. From 6 to 11 and 17 to 19 July, high concentrations of 1.2–4 nm particles are registered shortly after sunset for several hours, simultaneously at urban and suburban stations (see Fig. 2). BC, NO, and NO_2 concentrations also increase during that time (see Fig. 3). Therefore, these processes are probably related to local traffic emissions and the decrease of the mixing layer after sunset. On the other hand, from 12 to 14 July, high concentrations of sub-25 nm particles are also detected, but they only registered at the urban stations at around 23:00 UTC. These are sudden, shorter, and more intense, with concentrations greater than $10^5\,cm^{-3}$. They appear as intense bursts that last 1 h or less, with no subsequent growth. They are not accompanied by simultaneously high BC or NO concentrations; thus, they are not linked to traffic emissions, although NO_2 levels are significant. Furthermore, these episodes occur outside local traffic rush hours and are registered together with strong NE winds, which suggests that they might be transported from a stationary source and not formed locally. To better support this hypothesis, Fig. S6 shows PSM data together with wind direction and wind speed, showing that the episodes coincide with strong NE winds.

In order to determine the origin of these sub-25 nm particles, bivariate polar plots of concentration have been used to relate wind speed and direction measured at CIEMAT with total particle concentration of 1.2–2.5 nm particles, BC, NO_2, and NO measured at CSIC, analyzing daylight and nighttime periods separately (Fig. 9). These plots must be interpreted carefully, since the color scale only represents the average value for a given wind speed and direction. The results are consistent with what we previously stated; the highest nocturnal 1.2–2.5 nm particle concentrations are linked with strong winds from the NE direction. Air masses transported from this direction have the lowest BC levels and moderate NO_2 concentrations. NO concentrations are insignificant during the nighttime considering any direction, probably because of titration due to the high concentrations of O_3 observed during the daytime.

In the discussion paper, we pointed out the airport Adolfo Suárez Madrid–Barajas, located NE of the city, as a possible

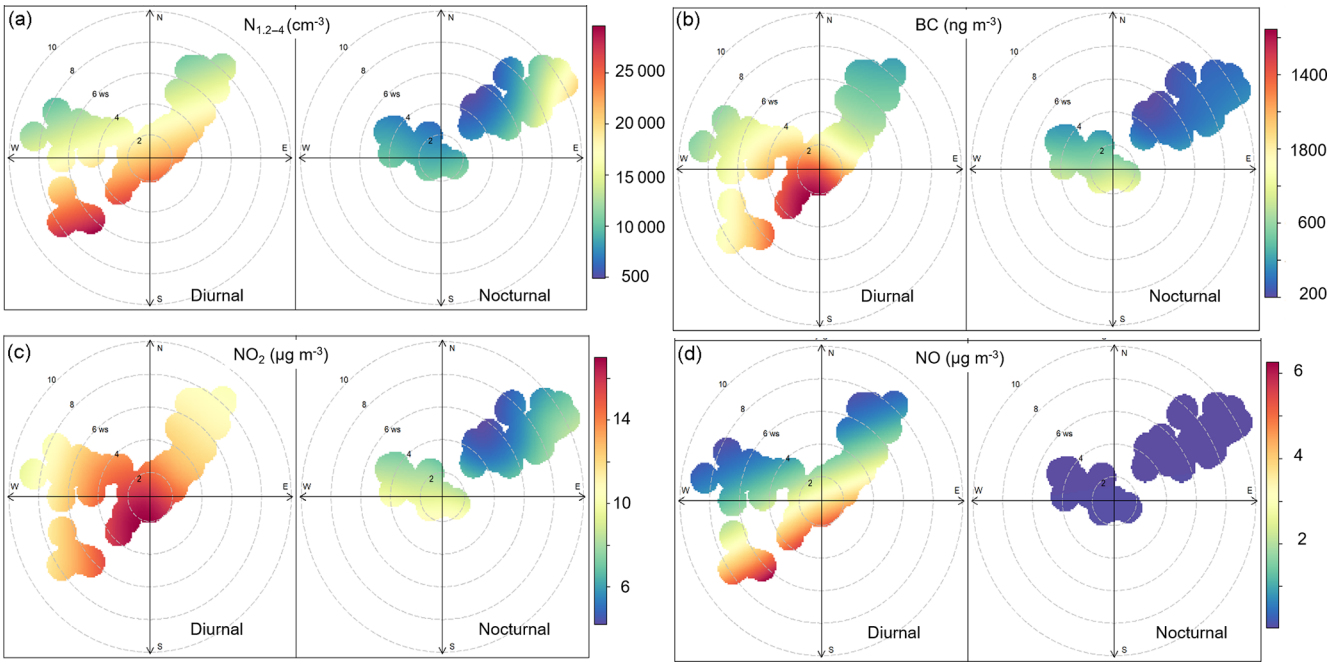

Figure 9. Bipolar plot of **(a)** total particle concentration in the size range 1.2–4 nm measured with the PSM, **(b)** black carbon (BC), **(c)** NO_2, and **(d)** NO concentrations at CSIC urban station using the wind data registered at CIEMAT. Daylight and nighttime hours are separated according to sunrise (05:00 UTC) and sunset (20:00 UTC). The data correspond to the period 11–15 July 2016.

source of these high UFP concentrations. However, the UFP peaks lasted for about 1 h on all days, whereas strong NE winds prevailed for a few hours. Moreover, the airport has flights all night; therefore, a longer period with high UFPs should be observed. Although other studies have linked aircraft emissions with nucleation bursts without growth (Cheung et al., 2011; Masiol et al., 2017), in this study we cannot affirm that the airport is the origin of these bursts. As mentioned before, these episodes were unexpected and were not the main focus of this study. To elucidate the origin of these UFP bursts, further research will be required.

4 Conclusions

We investigated the phenomenology of regional and secondary new particle formation (NPF) episodes in central Spain. To this end, we set up three supersites (an urban, an urban background, and a suburban site) 17 km apart in and around Madrid. We were able to characterize six NPF events, and, in all cases, the evolution of the particle size distribution (PSD) was very similar at all stations; around sunrise, nucleation-mode particles appear and start growing, and in the afternoon, a decline in particle sizes, i.e., shrinkage, is observed. The regional origin of the NPF is supported by the simultaneous variation in PSD in the nucleation mode, particle number concentrations, and growth and shrinkage rates. Furthermore, temporal evolutions of condensation and coagulation sinks were similar at all stations, having minimum values shortly before sunrise and increasing after dawn towards the maximum value after midday in the early afternoon. In spite of the 17 km scale and the simultaneous processes affecting particle number concentrations, the following relevant differences between urban and suburban stations were observed: (i) the urban stations presented larger formation rates as compared to the suburban stations, and (ii) in general, the sinks were higher at the urban stations.

Regarding the vertical soundings of the NPF events, we observed that, in the early morning, the vertical distribution of newly formed particles is differentiated into two layers. The lower layer (mixed layer – ML), in which convection is effective, is well-mixed and has a homogeneous PSD. This ML heightens throughout the day, as insolation is more pronounced, extending beyond the sounding limits around midday. NPF occurs throughout this ML, and GRs and concentrations are homogeneous. The upper layer is a stable residual layer (RL), in which particles formed or transported during the previous days prevail. In the RL, growth is inhibited or even completely restrained, compared with the growth of the same particles in the ML. Overall, the soundings demonstrate that particles are formed inside the ML, but they can prevail and be displaced and stored at upper levels and continue to evolve on following days.

In this campaign we could not measure during the earliest stages of NPF due to the safety requirements imposed on the balloon flights early in the morning. We think it is important for future work to carry out soundings during the

nucleation phase of the episodes. However, miniaturized instruments able to measure smaller particles would be needed and are not available at the present time. Carrying out these soundings would allow us to determine whether secondary NPF takes place throughout the ML or occurs at the surface and is transported upwards afterwards by convection. If the former is true, then locations with high ML could produce more secondary particles than we have considered, and they could affect a larger population or influence climate to a greater extent.

Additionally, a few nocturnal bursts of nucleation-mode particles were observed in the urban stations, and further research is needed to elucidate their origin.

We cannot determine whether the NPF episodes were triggered by the pollution generated in the city that extended to the region or caused by a broader phenomenon. Either way, it can be concluded that, in summer, the particle number concentrations are dominated by NPF in a wide area. The impact of traffic emissions on concentrations of UFPs is much smaller than that of NPF, even near the city center, where the pollution load is at the highest. This result is in line with other studies performed in cities from high-insolation regions (e.g., Kulmala et al., 2016). Given the extent of the episodes, the health effects of NPF can affect a vast number of people, considering that the Madrid metropolitan area, with more than 6 million inhabitants, is the most populated area in Spain and one of the most populated in Europe (UN, 2008). For this reason, we believe that the study of health effects related to newly formed particle inhalation is crucial.

Data availability. All data used in this study can be accessed here: https://doi.org/10.17632/x5gw4stjyb.1 (Pérez et al., 2018).

Supplement. The supplement related to this article is available online at: https://doi.org/10.5194/acp-18-16601-2018-supplement.

Author contributions. Data analysis was done by CC, NP and LD. CC, NP, LD, PP, VK, BT, NM, DB, RH, TP, MK, AA and XQ contributed to the discussion and interpretation of the results. CC and XQ wrote the manuscript. NP, CR, MEa, GT, HL, HE, YP, EM, MEs, FG, EA, EC, AS, BT, NM, DB, RH, KA, AA and XQ carried out the measurements. All the authors commented on the manuscript.

Competing interests. The authors declare that they have no conflict of interest.

Acknowledgements. This work was supported by the Spanish Ministry of Agriculture, Fishing, Food and Environment; the Ministry of Economy, Industry and Competitiveness; the Madrid City Council and Regional Government; FEDER funds under the project HOUSE (CGL2016-78594-R); the CUD of Zaragoza (project CUD 2016-05); the Government of Catalonia (AGAUR 2017 SGR44); and the Korean Ministry of Environment through "The Eco-Innovation project". The funding received by ERA-PLANET (http://www.era-planet.eu, last access: 16 November 2018), the trans-national project SMURBS (http://www.smurbs.eu, last access: 16 November 2018) (Grant agreement No. 689443), and the support of the Academy of Finland via the Center of Excellence in Atmospheric Sciences are acknowledged. These results are part of a project (ATM-GTP/ERC) that has received funding from the European Research Council (ERC) under the European Union's Horizon 2020 research and innovation program (Grant agreement No. 742206). The authors also acknowledge the Doctoral program of Atmospheric Sciences at the University of Helsinki (ATM-DP). Markku Kulmala acknowledges the support of the Academy of Finland via his Academy Professorship (no. 302958). We also thank the City Council of Majadahonda for logistic assistance, and the Instituto de Ciencias Agrarias, Instituto de Salud Carlos III, Alava Ingenieros, TSI, Solma Environmental Solutions, and Airmodus for their support.

Edited by: Paul Zieger
Reviewed by: two anonymous referees

References

Ahlm, L., Liu, S., Day, D. A., Russell, L. M., Weber, R., Gentner, D. R., Goldstein, A. H., Digangi, J. P., Henry, S. B., Keutsch, F. N., Vandenboer, T. C., Markovic, M. Z., Murphy, J. G., Ren, X., and Scheller, S.: Formation and growth of ultrafine particles from secondary sources in Bakersfield, California, J. Geophys. Res.-Atmos., 117, D00V08, https://doi.org/10.1029/2011JD017144, 2012.

Alonso-Blanco, E., Gómez-Moreno, F. J., Núñez, L., Pujadas, M., Cusack, M., and Artíñano, B.: Aerosol particle shrinkage event phenomenology in a South European suburban area during 2009–2015, Atmos. Environ., 160, 154–164, 2017.

Beddows, D. C. S., Harrison, R. M., Green, D. C., and Fuller, G. W.: Receptor modelling of both particle composition and size distribution from a background site in London, UK, Atmos. Chem. Phys., 15, 10107–10125, https://doi.org/10.5194/acp-15-10107-2015, 2015.

Boulon, J., Sellegri, K., Venzac, H., Picard, D., Weingartner, E., Wehrle, G., Collaud Coen, M., Bütikofer, R., Flückiger, E., Baltensperger, U., and Laj, P.: New particle formation and ultrafine charged aerosol climatology at a high altitude site in the Alps (Jungfraujoch, 3580 m a.s.l., Switzerland), Atmos. Chem. Phys., 10, 9333–9349, https://doi.org/10.5194/acp-10-9333-2010, 2010.

Boy, M. and Kulmala, M.: Nucleation events in the continental boundary layer: Influence of physical and meteorological parameters, Atmos. Chem. Phys., 2, 1–16, https://doi.org/10.5194/acp-2-1-2002, 2002.

Boy, M., Karl, T., Turnipseed, A., Mauldin, R. L., Kosciuch, E., Greenberg, J., Rathbone, J., Smith, J., Held, A., Barsanti, K., Wehner, B., Bauer, S., Wiedensohler, A., Bonn, B., Kulmala, M., and Guenther, A.: New particle formation in the Front Range of

the Colorado Rocky Mountains, Atmos. Chem. Phys., 8, 1577–1590, https://doi.org/10.5194/acp-8-1577-2008, 2008.

Brines, M., Dall'Osto, M., Beddows, D. C. S., Harrison, R. M., and Querol, X.: Simplifying aerosol size distributions modes simultaneously detected at four monitoring sites during SAPUSS, Atmos. Chem. Phys., 14, 2973–2986, https://doi.org/10.5194/acp-14-2973-2014, 2014.

Brines, M., Dall'Osto, M., Beddows, D. C. S., Harrison, R. M., Gómez-Moreno, F., Núñez, L., Artíñano, B., Costabile, F., Gobbi, G. P., Salimi, F., Morawska, L., Sioutas, C., and Querol, X.: Traffic and nucleation events as main sources of ultrafine particles in high-insolation developed world cities, Atmos. Chem. Phys., 15, 5929–5945, https://doi.org/10.5194/acp-15-5929-2015, 2015.

Buonanno, G. and Morawska, L.: Ultrafine particle emission of waste incinerators and comparison to the exposure of urban citizens, Waste Manage., 37, 75–81, 2015.

Carslaw, D. C. and Ropkins, K.: openair – an R package for air quality data analysis, Environ. Modell. Softw., 27–28, 52–61, 2012.

Charron, A. and Harrison, R. M.: Primary particle formation from vehicle emissions during exhaust dilution in the roadside atmosphere, Atmos. Environ., 37, 4109–4119, 2003.

Cheung, H. C., Morawska, L., and Ristovski, Z. D.: Observation of new particle formation in subtropical urban environment, Atmos. Chem. Phys., 11, 3823–3833, https://doi.org/10.5194/acp-11-3823-2011, 2011.

Coleman, B. K., Lunden, M. M., Destaillats, H., and Nazaroff, W. W.: Secondary organic aerosol from ozone-initiated reactions with terpene-rich household products, Atmos. Environ., 42, 8234–8245, 2008.

Costabile, F., Birmili, W., Klose, S., Tuch, T., Wehner, B., Wiedensohler, A., Franck, U., König, K., and Sonntag, A.: Spatio-temporal variability and principal components of the particle number size distribution in an urban atmosphere, Atmos. Chem. Phys., 9, 3163–3195, https://doi.org/10.5194/acp-9-3163-2009, 2009.

Crespí, S. N., Artíñano, B., and Cabal, H.: Synoptic classification of the mixed-layer height evolution, J. Appl. Meteorol., 34, 1668–1677, 1995.

Cusack, M., Pérez, N., Pey, J., Alastuey, A., and Querol, X.: Variability of submicrometer particle number size distributions in the western Mediterranean regional background, Tellus B, 65, 19243, https://doi.org/10.3402/tellusb.v65i0.19243, 2013a.

Cusack, M., Alastuey, A., and Querol, X.: Case studies of new particle formation and evaporation processes in the western Mediterranean regional background, Atmos. Environ., 81, 651–659, 2013b.

Dall'Osto, M., Beddows, D. C. S., Pey, J., Rodriguez, S., Alastuey, A., Harrison, R. M., and Querol, X.: Urban aerosol size distributions over the Mediterranean city of Barcelona, NE Spain, Atmos. Chem. Phys., 12, 10693–10707, https://doi.org/10.5194/acp-12-10693-2012, 2012.

Dall'Osto, M., Querol, X., Alastuey, A., O'Dowd, C., Harrison, R. M., Wenger, J., and Gómez-Moreno, F. J.: On the spatial distribution and evolution of ultrafine particles in Barcelona, Atmos. Chem. Phys., 13, 741–759, https://doi.org/10.5194/acp-13-741-2013, 2013.

Dal Maso, M., Kulmala, M., Riipinen, I., Wagner, R., Hussein, T., Aalto, P. P., and Lehtinen, K. E. J.: Formation and growth of fresh atmospheric aerosols: eight years of aerosol size distribution data from SMEAR II, Hyytiälä, Finland, Boreal Environ. Res., 10, 323–336, 2005.

El Haddad, I., D'Anna, B., Temime-Roussel, B., Nicolas, M., Boreave, A., Favez, O., Voisin, D., Sciare, J., George, C., Jaffrezo, J.-L., Wortham, H., and Marchand, N.: Towards a better understanding of the origins, chemical composition and aging of oxygenated organic aerosols: case study of a Mediterranean industrialized environment, Marseille, Atmos. Chem. Phys., 13, 7875–7894, https://doi.org/10.5194/acp-13-7875-2013, 2013.

García, M. I., Rodríguez, S., González, Y., and García, R. D.: Climatology of new particle formation at Izaña mountain GAW observatory in the subtropical North Atlantic, Atmos. Chem. Phys., 14, 3865–3881, https://doi.org/10.5194/acp-14-3865-2014, 2014.

Gómez-Moreno, F. J., Pujadas, M., Plaza, J., Rodríguez-Maroto, J. J., Martínez-Lozano, P., and Artíñano, B.: Influence of seasonal factors on the atmospheric particle number concentration and size distribution in Madrid, Atmos. Environ., 45, 3199–3180, 2011.

Graus, M., Muller, M., and Hansel, A.: High Resolution PTR-TOF: Quantification and Formula Confirmation of VOC in Real Time, J. Am. Soc. Mass Spectr., 21, 1037–1044, 2010.

Hofman, J., Staelensa, J., Cordell, R., Stroobants, C., Zikova, N., Hama, S. M. L., Wyche, K. P., Kosf, G. P. A., Van Der Zeeg, S., Smallbone, K. L., Weijers, E. P., and Monks, P. S.: Ultrafine particles in four European urban environments: Results from a new continuous long-term monitoring network, Atmos. Environ., 136, 68–81, 2016.

Hudda, N., Gould, T., Hartin, K., Larson, T. V., and Fruin, S. A.: Emissions from an International Airport Increase Particle Number Concentrations 4-fold at 10 km Downwind, Environ. Sci. Technol., 48, 6628–6635, 2014.

Hussein, T., Dal Maso, M., Petäjä, T., Koponen, I., Paatero, P., Aalto, P., Hämeri, K., and Kulmala, M.: Evaluation of an automatic algorithm for fitting the particle number size distributions, Boreal Environ. Res., 10, 337–355, 2005.

Hussein, T., Martikainen, J., Junninen, H., Sogacheva, L., Wagner, R., Dal Maso, M., Riipinen, I., Aalto, P. P., and Kulmala, M.: Observation of regional new particle formation in the urban atmosphere, Tellus B, 60, 509–521, https://doi.org/10.1111/j.1600-0889.2008.00365.x, 2008.

Johnson, G. R., Juwono, A. M., Friend, A. J., Cheung, H.-C., Stelcer, E., Cohen, D., Ayoko, G. A., and Morawska, L.: Relating urban airborne particle concentrations to shipping using carbon based elemental emission ratios, Atmos. Environ., 95, 525–536, 2014.

Kecorius, S., Kivekäs, N., Kristenssond, A., Tuch, T., Covert, D. S., Birmili, W. Lihavainen, H., Hyvärinen, A.-P., Martinsson, J., Sporre, M. K., Swietlicki, E., Wiedensohler, A., and Ulevicius, V.: Significant increase of aerosol number concentrations in air masses crossing a densely trafficked sea area, Oceanologia, 58, 1–12, 2016.

Keuken, M. P., Moerman, M., Zandveld, P., Henzing, J. S., and Hoek, G.: Total and size-resolved particle number and black carbon concentrations in urban areas near Schiphol airport (the Netherlands), Atmos. Environ., 104, 132–142, 2015.

Kirkby, J., Duplissy, J., Sengupta, K., Frege, C., Gordon, H., Williamson, C., Heinritzi, M., Simon, M., Yan, C., Almeida, J., Trostl, J., Nieminen, T., Ortega, I. K., Wagner, R., Adamov, A.,

Amorim, A., Bernhammer, A. K., Bianchi, F., Breitenlechner, M., Brilke, S., Chen, X., Craven, J., Dias, A., Ehrhart, S., Flagan, R. C., Franchin, A., Fuchs, C., Guida, R., Hakala, J., Hoyle, C. R., Jokinen, T., Junninen, H., Kangasluoma, J., Kim, J., Krapf, M., Kurten, A., Laaksonen, A., Lehtipalo, K., Makhmutov, V., Mathot, S., Molteni, U., Onnela, A., Perakyla, O., Piel, F., Petaja, T., Praplan, A. P., Pringle, K., Rap, A., Richards, N. A. D., Riipinen, I., Rissanen, M. P., Rondo, L., Sarnela, N., Schobesberger, S., Scott, C. E., Seinfeld, J. H., Sipila, M., Steiner, G., Stozhkov, Y., Stratmann, F., Tomé, A., Virtanen, A., Vogel, A. L., Wagner, A. C., Wagner, P. E., Weingartner, E., Wimmer, D., Winkler, P. M., Ye, P., Zhang, X., Hansel, A., Dommen, J., Donahue, N. M., Worsnop, D. R., Baltensperger, U., Kulmala, M., Carslaw, K. S., and Curtius, J.: Ion-induced nucleation of pure biogenic particles, Nature, 533, 521–526, https://doi.org/10.1038/nature17953, 2016.

Kittelson, D. B., Watts, W. F., and Johnson, J. P.: On-road and laboratory evaluation of combustion aerosols – Part 1: Summary of diesel engine results, J. Aerosol Sci., 37, 913–930, 2006.

Kontkanen, J., Lehtipalo, K., Ahonen, L., Kangasluoma, J., Manninen, H. E., Hakala, J., Rose, C., Sellegri, K., Xiao, S., Wang, L., Qi, X., Nie, W., Ding, A., Yu, H., Lee, S., Kerminen, V.-M., Petäjä, T., and Kulmala, M.: Measurements of sub-3 nm particles using a particle size magnifier in different environments: from clean mountain top to polluted megacities, Atmos. Chem. Phys., 17, 2163–2187, https://doi.org/10.5194/acp-17-2163-2017, 2017.

Kulmala, M. and Kerminen, V.-M.: On the formation and growth of atmospheric nanoparticles, Atmos. Res., 90, 132–150, 2008.

Kulmala, M., Pirjola, L., and Mäkelä, J. M.: Stable Sulphate Clusters as a Source of New Atmospheric Particles, Nature, 404, 66–69, 2000.

Kulmala, M., Vehkamehk, H., Pet, P. T., Dal Maso, M., Lauri, A., Kerminen, V.-M., Birmili, W., and McMurry, P.: Formation and growth rates of ultrafine atmospheric particles: a review of observations, J. Aerosol Sci., 35, 143–176, 2004.

Kulmala, M., Petäjä, T., Nieminen, T., Sipilä, M., Manninen, H. E., Lehtipalo, K., Dal Maso, M., Aalto, P. P., Junninen, H., Paasonen, P., Riipinen, I., Lehtinen, K. E. J., Laaksonen, A., and Kerminen, V.-M.: Measurement of the nucleation of atmospheric aerosol particles, Nat. Protoc., 7, 1651–1667, 2012.

Kulmala, M., Luoma, K., Virkkula, A., Petäjä, T., Paasonen, P., Kerminen, V.M., Nie, W., Qi, X., Shen, Y., Chi, X., and Ding, A.: On the mode-segregated aerosol particle number concentration load: Contributions of primary and secondary particles in Hyytiälä and Nanjing, Boreal Environ. Res., 21, 319–331, 2016.

Kumar, P. and Morawska, L.: Recycling Concrete: An Undiscovered Source of Ultrafine Particles, Atmos. Environ, 90, 51–58, 2014.

Kumar, P., Morawska, L., Birmili, W., Paasonen, P., Hu, M., Kulmala, M., Harrison, R. M., Norford, L., and Britter, R.: Ultrafine particles in cities, Environ. Int., 66, 1–10, 2014.

Lee, H.-K., Hwang, I.-K., and Ahn, K.-H.: Development and Evaluation of Hy-CPC, Particle and Aerosol Research, 10, 93–97, 2014.

Lee, H.-K., Eun, H.-R., Lee, G.-H., and Ahn, K.-H.: Development and evaluation of Hy-SMPS, Particle and Aerosol Research, 11, 57–61, 2015.

Ma, N. and Birmili, W.: Estimating the contribution of photochemical particle formation to ultrafine particle number averages in an urban atmosphere, Sci. Total Environ., 512–513, 154–166, 2015.

Manninen, H. E., Nieminen, T., Asmi, E., Gagné, S., Häkkinen, S., Lehtipalo, K., Aalto, P., Vana, M., Mirme, A., Mirme, S., Hõrrak, U., Plass-Dülmer, C., Stange, G., Kiss, G., Hoffer, A., Töro, N., Moerman, M., Henzing, B., de Leeuw, G., Brinkenberg, M., Kouvarakis, G. N., Bougiatioti, A., Mihalopoulos, N., O'Dowd, C., Ceburnis, D., Arneth, A., Svenningsson, B., Swietlicki, E., Tarozzi, L., Decesari, S., Facchini, M. C., Birmili, W., Sonntag, A., Wiedensohler, A., Boulon, J., Sellegri, K., Laj, P., Gysel, M., Bukowiecki, N., Weingartner, E., Wehrle, G., Laaksonen, A., Hamed, A., Joutsensaari, J., Petäjä, T., Kerminen, V.-M., and Kulmala, M.: EUCAARI ion spectrometer measurements at 12 European sites – analysis of new particle formation events, Atmos. Chem. Phys., 10, 7907–7927, https://doi.org/10.5194/acp-10-7907-2010, 2010.

Masiol, M., Harrison, R. M., Vu, T. V., and Beddows, D. C. S.: Sources of sub-micrometre particles near a major international airport, Atmos. Chem. Phys., 17, 12379–12403, https://doi.org/10.5194/acp-17-12379-2017, 2017.

Minguillón, M. C., Brines, M., Pérez, N., Reche, C., Pandolfi, M., Fonseca, A. S., Amato, F., Alastuey, A., Lyasota, A., Codina, B., Lee, H.-K., Eun, H.-R., Ahn, K.-H., and Querol, X.: New particle formation at ground level and in the vertical column over the Barcelona area, Atmos. Res., 164–165, 118–130, 2015.

Nie, W., Ding, A. J., Wang, T., Kerminen, V.-M., George, C., Xue, L. K., Wang, W. X., Zhang, Q. Z., Petäjä, T., Qi, X. M., Gao, X. M., Wang, X. F., Yang, X. Q., Fu, C. B., and Kulmala, M.: Polluted dust promotes new particle formation and growth, Sci. Rep.-UK, 4, 6634, https://doi.org/10.1038/srep06634, 2014.

O'Dowd, C., Monahan, C., and Dall'Osto, M.: On the occurrence of open ocean particle production and growth events, Geophys. Res. Lett., 37, L19805, https://doi.org/10.1029/2010GL044679, 2010.

Paasonen, P., Kupiainen, K., Klimont, Z., Visschedijk, A., Denier van der Gon, H. A. C., and Amann, M.: Continental anthropogenic primary particle number emissions, Atmos. Chem. Phys., 16, 6823–6840, https://doi.org/10.5194/acp-16-6823-2016, 2016.

Pérez, N., Reche, C., Ealo, M., Titos, G., Lee, H. K., Eun, H.-R., Park, Y.-H., Mantilla, E., Escudero, M., Gómez-Moreno, F. J., Alonso-Blanco, E., Coz, E., Saiz-Lopez, A., Beddows, D., Harrison, R. M., Ahn, K.-H., Alastuey, A., and Querol, X.: O3, UFP and VOCs field campaign in Madrid, July 2016, Mendeley Data, v1 https://doi.org/10.17632/x5gw4stjyb.1, 2018.

Pey, J., Rodríguez, S., Querol, X., Alastuey, A., Moreno, T., Putaud, J. P., and Van Dingenen, R.: Variations of urban aerosols in the western Mediterranean, Atmos. Environ., 42, 9052–9062, 2008.

Pey, J., Querol, X., Alastuey, A., Rodríguez, S., Putaud, J. P., and Van Dingenen, R.: Source Apportionment of urban fine and ultrafine particle number concentration in a Western Mediterranean city, Atmos. Environ., 43, 4407–4415, 2009.

Plaza, J., Pujadas, M., and Artíñano, B.: Formation and Transport of the Madrid Ozone Plume, J. Air Waste Manage., 47, 766–774, 1997.

Qian, S., Sakurai, H., and McMurry, P. H.: Characteristics of regional nucleation events in urban East St. Louis, Atmos. Environ., 41, 4119–4127, 2007.

Querol, X., Gangoiti, G., Mantilla, E., Alastuey, A., Minguillón, M. C., Amato, F., Reche, C., Viana, M., Moreno, T., Karanasiou, A., Rivas, I., Pérez, N., Ripoll, A., Brines, M., Ealo, M., Pandolfi, M., Lee, H.-K., Eun, H.-R., Park, Y.-H., Escudero, M., Beddows, D., Harrison, R. M., Bertrand, A., Marchand, N., Lyasota, A., Codina, B., Olid, M., Udina, M., Jiménez-Esteve, B., Soler, M. R., Alonso, L., Millán, M., and Ahn, K.-H.: Phenomenology of high-ozone episodes in NE Spain, Atmos. Chem. Phys., 17, 2817–2838, https://doi.org/10.5194/acp-17-2817-2017, 2017.

Querol, X., Alastuey, A., Gangoiti, G., Perez, N., Lee, H. K., Eun, H. R., Park, Y., Mantilla, E., Escudero, M., Titos, G., Alonso, L., Temime-Roussel, B., Marchand, N., Moreta, J. R., Revuelta, M. A., Salvador, P., Artíñano, B., García dos Santos, S., Anguas, M., Notario, A., Saiz-Lopez, A., Harrison, R. M., Millán, M., and Ahn, K.-H.: Phenomenology of summer ozone episodes over the Madrid Metropolitan Area, central Spain, Atmos. Chem. Phys., 18, 6511–6533, https://doi.org/10.5194/acp-18-6511-2018, 2018.

Reche, C., Querol, X., Alastuey, A., Viana, M., Pey, J., Moreno, T., Rodríguez, S., González, Y., Fernández-Camacho, R., de la Rosa, J., Dall'Osto, M., Prévôt, A. S. H., Hueglin, C., Harrison, R. M., and Quincey, P.: New considerations for PM, Black Carbon and particle number concentration for air quality monitoring across different European cities, Atmos. Chem. Phys., 11, 6207–6227, https://doi.org/10.5194/acp-11-6207-2011, 2011.

Robinson, A. L., Donahue, N. M., Shrivastava, M. K., Weitkamp, E. A., Sage, A. M., Grieshop, A. P., Lane, T. E., Pierce, J. R., and Pandis, S. N.: Rethinking organic aerosols: semivolatile emissions and photochemical aging, Science 31, 1259–1262, 2007.

Rönkkö, T., Kuuluvainen, H., Karjalainen, P., Keskinen, J., Hillamo, R., Niemi, J. V, Pirjola, L., Timonen, H.J., Saarikoski, S., Saukko, E., Järvinen, A., Silvennoinen, H., Rostedt, A., Olin, M., Yli-Ojanperä, J., Nousiainen, P., Kousa, A., and Dal Maso, M.: Traffic is a major source of atmospheric nanocluster aerosol, P. Natl. Acad. Sci. USA, 114, 7549–7554, https://doi.org/10.1073/pnas.1700830114, 2017.

Saiz-Lopez, A., Borge, R., Notario, A., Adame, J. A., De la Paz, D., Querol, X., Artíñano, B., Gomez-Moreno, F. J., and Cuevas, C. A.: Unexpected increase in the oxidation capacity of the urban atmosphere of Madrid, Spain, Sci. Rep., 7, 45956, https://doi.org/10.1038/srep45956, 2017.

Salma, I., Borsos T., Nemeth Z., Weidiger T., Aalto P., and Kulmala M.: Comparative study of ultrafine atmospheric aerosol within a city, Atmos. Environ., 92, 154–161, 2014.

Salma, I., Németh, Z., Kerminen, V.-M., Aalto, P., Nieminen, T., Weidinger, T., Molnár, Á., Imre, K., and Kulmala, M.: Regional effect on urban atmospheric nucleation, Atmos. Chem. Phys., 16, 8715–8728, https://doi.org/10.5194/acp-16-8715-2016, 2016.

Salvador, P., Artíñano, B., Viana, M., Alastuey, A., and Querol, X.: Multicriteria approach to interpret the variability of the levels of particulate matter and gaseous pollutants in the Madrid metropolitan area, during the 1999–2012 period, Atmos. Environ., 109, 205–216, 2015.

Sellegri, K., Laj, P., Venzac, H., Boulon, J., Picard, D., Villani, P., Bonasoni, P., Marinoni, A., Cristofanelli, P., and Vuillermoz, E.: Seasonal variations of aerosol size distributions based on long-term measurements at the high altitude Himalayan site of Nepal Climate Observatory-Pyramid (5079 m), Nepal, Atmos. Chem. Phys., 10, 10679–10690, https://doi.org/10.5194/acp-10-10679-2010, 2010.

Sipilä, M., Berndt, T., Petaja, T., Brus, D., Vanhanen, J., Stratmann, F., Patokoski, J., Mauldin, R. L., Hyvärinen, A. P., Lihavainen, H., and Kulmala, M.: The role of sulfuric acid in atmospheric nucleation, Science, 327, 1243–1246, https://doi.org/10.1126/science.1180315, 2010.

Shi, J. P. and Harrison, R. M.: Investigation of ultrafine particle formation during diesel exhaust dilution, Environ. Sci. Technol., 33, 3730–3736, 1999.

Shi, J. P., Mark, D., and Harrison, R. M.: Characterization of particles from a current technology heavy-duty diesel engine, Environ. Sci. Technol., 34, 748–755, 2000.

Skrabalova, L., Zikova, N., and Zdimal, V.: Shrinkage of newly formed particles in an urban environment, Aerosol Air Qual. Res., 15, 1313–1324, 2015.

Stolzenburg, M. R., McMurry, P. H., Sakurai, H., Smith, J. N., Lee, M. R., Eisele, F. L., and Clement, C. F.: Growth rates of freshly nucleated atmospheric particles in Atlanta, J. Geophys. Res., 110, D22S05, https://doi.org/10.1029/2005JD005935, 2005.

Stratmann, F., Siebert, H., Spindler, G., Wehner, B., Althausen, D., Heintzenberg, J., Hellmuth, O., Rinke, R., Schmieder, U., Seidel, C., Tuch, T., Uhrner, U., Wiedensohler, A., Wandinger, U., Wendisch, M., Schell, D., and Stohl, A.: New-particle formation events in a continental boundary layer: first results from the SATURN experiment, Atmos. Chem. Phys., 3, 1445–1459, https://doi.org/10.5194/acp-3-1445-2003, 2003.

Stull, R. B.: An introduction to boundary layer meteorology, Kluwer Academic Publishers, Dordrecht, the Netherlands, Boston, USA and London, UK, 1988.

Tröstl, J., Chuang, W. K., Gordon, H., Heinritzi, M., Yan, C., Molteni, U., Ahlm, L., Frege, C., Bianchi, F., Wagner, R., Simon, M., Lehtipalo, K., Williamson, C., Craven, J. S., Duplissy, J., Adamov, A., Almeida, J., Bernhammer, A. K., Breitenlechner, M., Brilke, S., Dias, A., Ehrhart, S., Flagan, R. C., Franchin, A., Fuchs, C., Guida, R., Gysel, M., Hansel, A., Hoyle, C. R., Jokinen, T., Junninen, H., Kangasluoma, J., Keskinen, H., Kim, J., Krapf, M., Kürten, A., Laaksonen, A., Lawler, M., Leiminger, M., Mathot, S., Möhler, O., Nieminen, T., Onnela, A., Petäjä, T., Piel, F. M., Miettinen, P., Rissanen, M. P., Rondo, L., Sarnela, N., Schobesberger, S., Sengupta, K., Sipilä, M., Smith, J. N., Steiner, G., Tomè, A., Virtanen, A., Wagner, A. C., Weingartner, E., Wimmer, D., Winkler, P. M., Ye, P., Carslaw, K. S., Curtius, J., Dommen, J., Kirkby, J., Kulmala, M., Riipinen, I., Worsnop, D. R., Donahue, N. M., and Baltensperger, U.: The role of low-volatility organic compounds in initial particle growth in the atmosphere, Nature, 533, 527–531, https://doi.org/10.1038/nature18271, 2016.

Uhrner, U., von Lowis, S., Vehkamaki, H., Wehner, B., Brasel, S., Hermann, M., Stratmann, F., Kulmala, M., and Wiedensohler, A.: Dilution and aerosol dynamics within a diesel car exhaust plume – CFD simulations of on-road conditions, Atmos. Environ., 41, 7440–7461, 2007.

United Nations: World Urbanization Prospects (2007 revision), Department of Economic and Social Affairs, available at: https://www.un.org/esa/population/publications/wup2007/2007WUP_Highlights_web.pdf (last access: 16 November 2018), 2008.

Vakkari, V., Laakso, H., Kulmala, M., Laaksonen, A., Mabaso, D., Molefe, M., Kgabi, N., and Laakso, L.: New particle formation events in semi-clean South African savannah, Atmos. Chem. Phys., 11, 3333–3346, https://doi.org/10.5194/acp-11-3333-2011, 2011.

von Bismarck-Osten, C., Birmili, W., Ketzel, M., Massling, A., Petäjä, T., and Weber, S.: Characterization of parameters influencing the spatio-temporal variability of urban particle number size distributions in four European cities, Atmos. Environ., 77, 415–429, 2013.

Wang, N., Sun, X., Chen, J., and Li, X.: Sci. Heterogeneous Nucleation of Trichloroethylene Ozonation Products in the Formation of New Fine Particles, Sci. Rep.-UK, 7, 42600, https://doi.org/10.1038/srep42600, 2017.

Wegner, T., Hussein, T., Hämeri, K., Vesala, T., Kulmala, M., and Weber, S.: Properties of aerosol signature size distributions in the urban environment as derived by cluster analysis, Atmos. Environ., 61, 350–360, 2012.

Wehner, B. and Wiedensohler, A.: Long term measurements of submicrometer urban aerosols: statistical analysis for correlations with meteorological conditions and trace gases, Atmos. Chem. Phys., 3, 867–879, https://doi.org/10.5194/acp-3-867-2003, 2003.

Wehner, B., Siebert, H., Stratmann, F., Tuch, T., Wiedensohler, A., Petäjä, T., Dal Maso, M., and Kulmala, M.: Horizontal homogeneity and vertical extent of new particle formation events, Tellus, 59B, 362–371, 2007.

Wehner, B., Siebert, H., Ansmann, A., Ditas, F., Seifert, P., Stratmann, F., Wiedensohler, A., Apituley, A., Shaw, R. A., Manninen, H. E., and Kulmala, M.: Observations of turbulence-induced new particle formation in the residual layer, Atmos. Chem. Phys., 10, 4319–4330, https://doi.org/10.5194/acp-10-4319-2010, 2010.

Wiedensohler, A., Wehner, B., and Birmili, W.: Aerosol number concentrations and size distributions at mountain-rural, urban-influenced rural, and urban-background sites in Germany, J. Aerosol Med., 15, 237–243, 2002.

Woo, K. S., Chen, D. R., Pui, D. Y. H., and McMurry, P. H.: Measurement of Atlanta aerosol size distributions: observations of ultrafine particle events, Aerosol Sci. Tech., 34, 75–87, 2001.

Yao, X., Choi, M. Y., Lau, N. T., Lau, A. P. S., Chan, C. K., and Fang, M.: Growth and shrinkage of new particles in the atmosphere in Hong Kong, Aerosol Sci. Tech., 44, 639–650, 2010.

Young, L.-H., Lee, S.-H., Kanawade, V. P., Hsiao, T.-C., Lee, Y. L., Hwang, B.-F., Liou, Y.-J., Hsu, H.-T., and Tsai, P.-J.: New particle growth and shrinkage observed in subtropical environments, Atmos. Chem. Phys., 13, 547–564, https://doi.org/10.5194/acp-13-547-2013, 2013.